




Strip-based digital image registration for distortion minimization and robust eye motion measurement from scanned ophthalmic imaging systems: supplement

MIN ZHANG,^{1,5,6} ELENA GOFAS-SALAS,^{1,5}  BIANCA T. LEONARD,¹ YUHUA RUI,^{1,2} VALERIE C. SNYDER,¹ HOPE M. REECHER,¹ PEDRO MECÊ,¹  AND ETHAN A. ROSSI^{1,3,4,7} 

¹Department of Ophthalmology, University of Pittsburgh School of Medicine, Pittsburgh, PA 15213, USA

²Eye center of Xiangya Hospital, Central South University; Hunan Key Laboratory of Ophthalmology; Changsha, Hunan 410008, China

³Department of Bioengineering, University of Pittsburgh Swanson School of Engineering, Pittsburgh, PA 15261, USA

⁴McGowan Institute for Regenerative Medicine, University of Pittsburgh, Pittsburgh, Pennsylvania 15260, USA

⁵Denotes that each of these authors contributed equally to this work

⁶miz62@pitt.edu

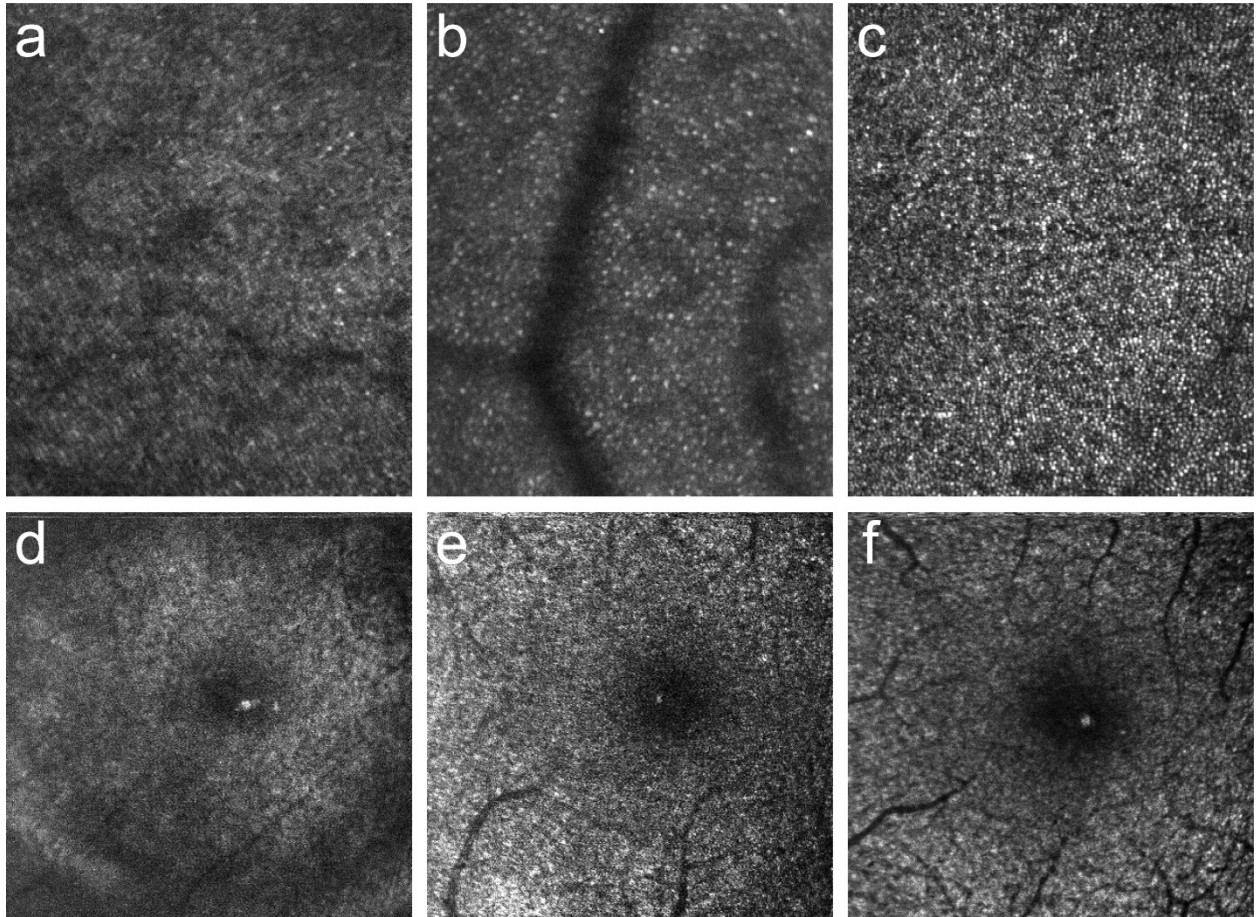
⁷rossiea@pitt.edu

This supplement published with The Optical Society on 25 March 2021 by The Authors under the terms of the [Creative Commons Attribution 4.0 License](https://creativecommons.org/licenses/by/4.0/) in the format provided by the authors and unedited. Further distribution of this work must maintain attribution to the author(s) and the published article's title, journal citation, and DOI.

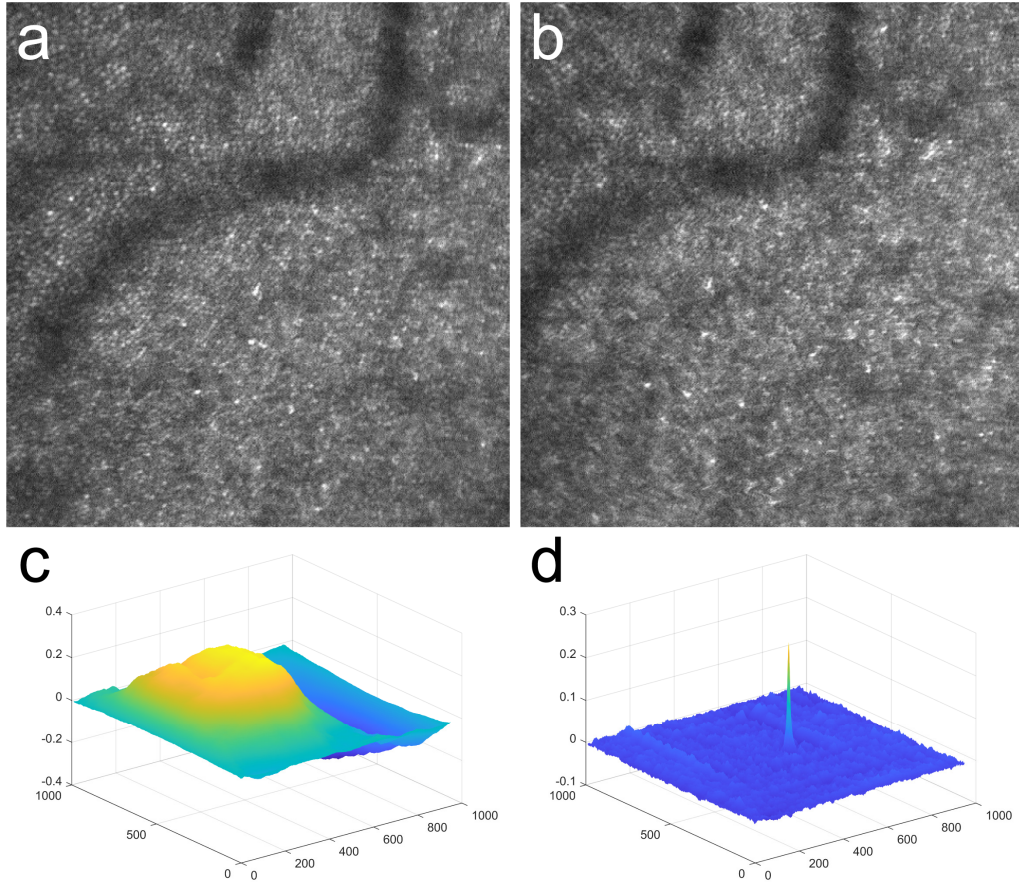
Supplement DOI: <https://doi.org/10.6084/m9.figshare.14221700>

Parent Article DOI: <https://doi.org/10.1364/BOE.418070>

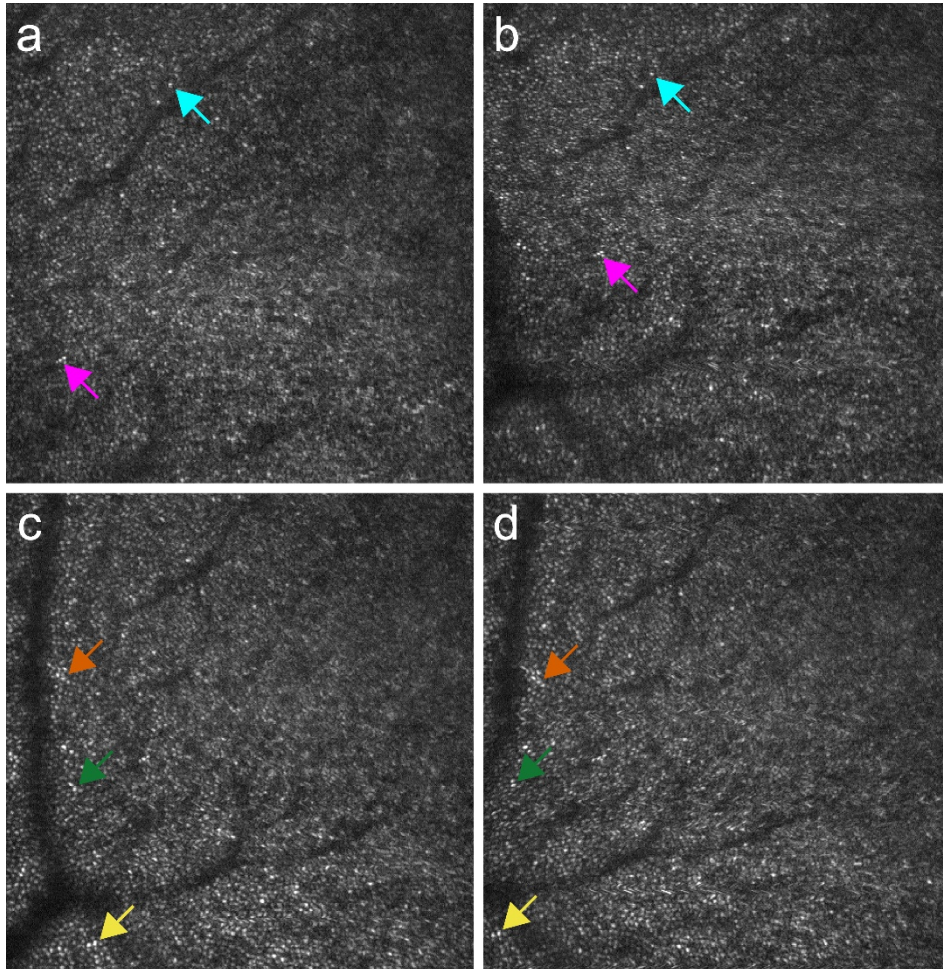
Supplementary Figures



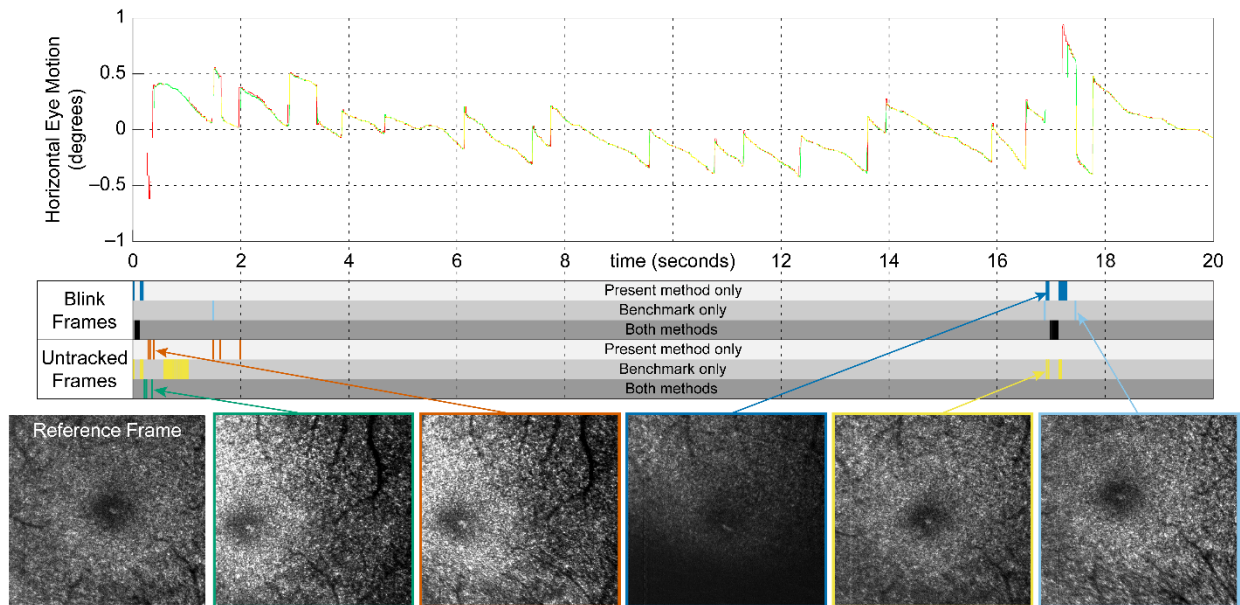
Supplementary Figure S1. Representative examples of range of image quality in test data. Top row shows examples from AOSLO of low (a), medium (b) and high quality (c) frames, while bottom row shows example of low (d), medium (e) and high quality (f) frames for TSLO data. Image height is 1.5° for AOSLO images and 5° degrees for TSLO.



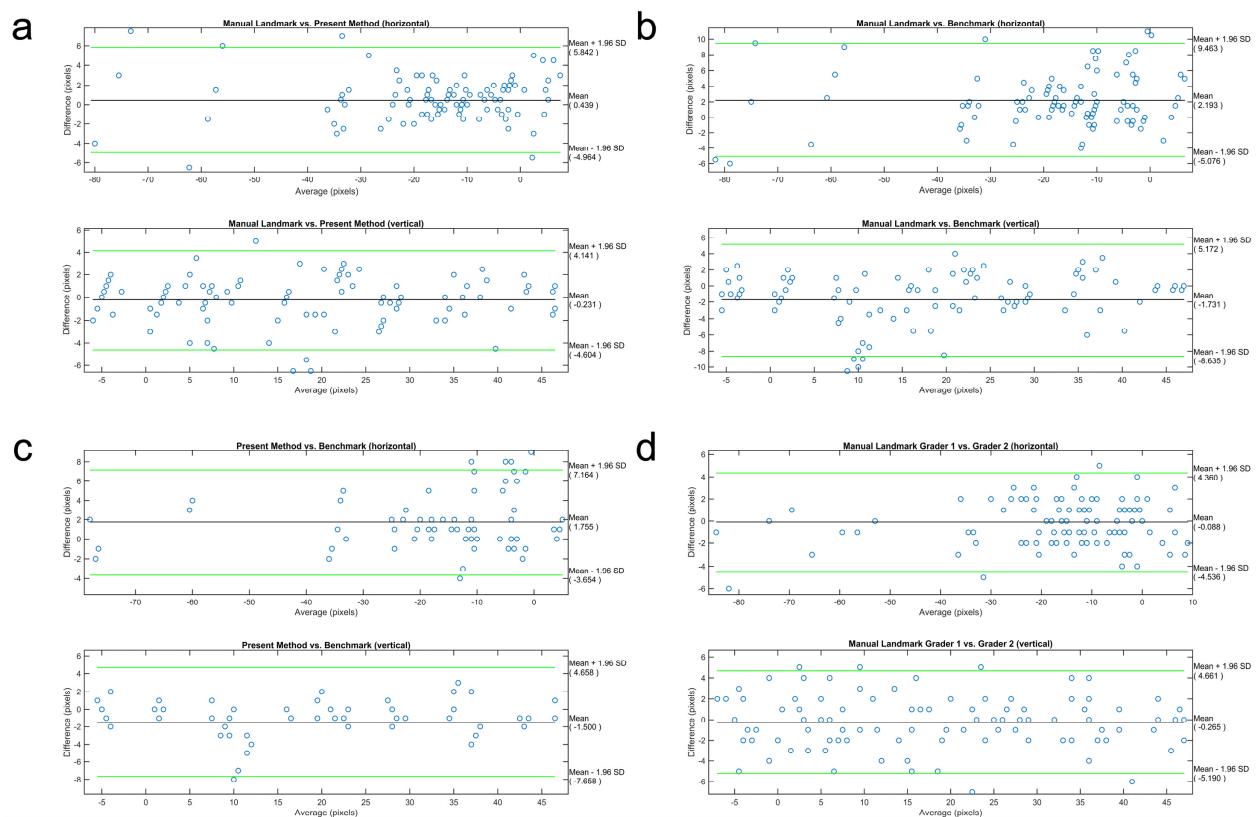
Supplementary Figure S2. Comparing the NCC with and without the Gaussian filtering and CLAHE pre-processing steps. Reference frame (a) and target frame (b). The NCC of (a) and (b) without pre-processing leads to a broad distribution with a poorly defined peak (c). After pre-processing (d), the NCC shows a sharp well-defined peak leading to a more accurate determination of its position. Images are from AOSLO.



Supplementary Figure S3. Examples of two common distortions seen in scanned systems that are highly visible. Two consecutive raw frames from an AOSLO image sequence are shown in the top and bottom row. The preceding frame before each visible distortion is shown on the left, while the highly distorted frames are shown on the right. The cyan and magenta arrows in (a) denote the positions of a few bright cones that are clearly visible in each image. The compression distortion in (b) causes the positions of these cones to appear closer to one another than in (a); also note that the cones in between the arrows are compressed into ellipses. In (c) and (d) the orange, green and yellow arrows again point to bright cones clearly visible in each image. In (c) the orange, green and yellow arrows are arrayed from top left to bottom right, respectively, while in (d) they are arrayed in the opposite direction. This is due to the shearing distortion in the image; also note that the cones appear elliptical across much of the lower portion of the image. When manually selecting a reference frame, we selected frames that were free from visible distortions such as the compression (b) and shearing (d) shown here. Image height is $\sim 1.5^\circ$.



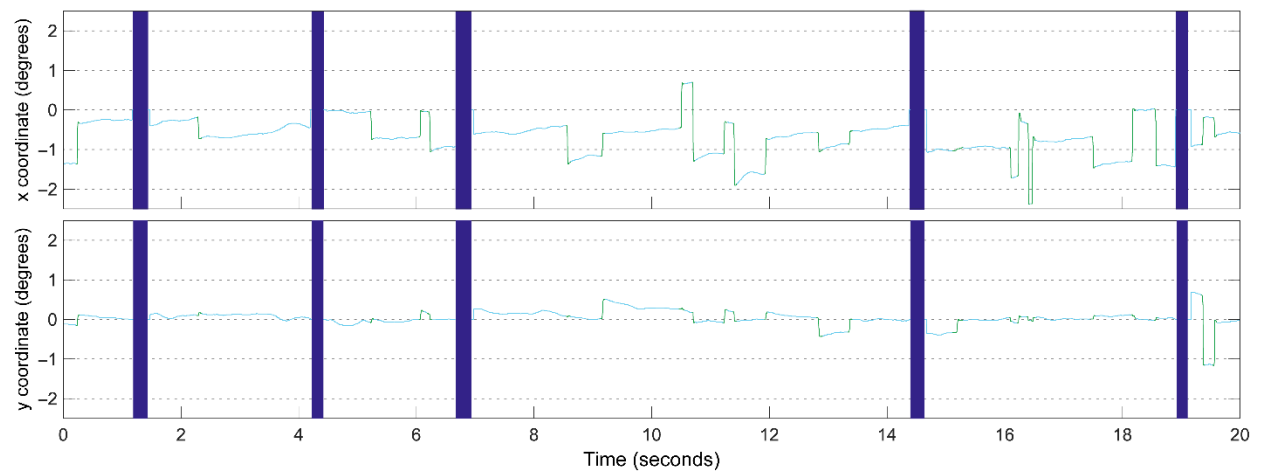
Supplementary Figure S4. Comparison of frames detected as blinks and untracked frames. Eye traces (upper plot) from TSLO, generated when selecting the same reference frame (lower left) are overlaid from the present method (green) and benchmark (red). Positions of overlap are shown in yellow. The corresponding timeline below displays the timing of the blink and untracked frames detected for each method. While both algorithms marked some of the same frames as blinks (black frames), the present method also marks some additional frames before and after each of these periods as blinks (dark blue frames). These included frames where the eye was partially opened, and the intensity fell below the threshold (e.g. image outlined in dark blue). These frames are untracked by the benchmark but not marked as blinks (see yellow frames around black blink frames around 1 sec and 17 secs). Some highly saturated frames with large motion were discarded by both methods (green frames). The benchmark left untracked a few frames that the present method did not (cyan frames; e.g. image outlined in cyan). The present method discarded some frames that the benchmark did not, including some highly distorted frames (e.g. image outlined in orange).



Supplementary Figure S5. Bland-Altman plots show agreement between present method, benchmark, and manual graders. The average difference was less than 0.5 pixels in either direction between the manual landmark and present method (a), while the difference was larger, around 2 pixels, on average, for the manual landmark versus the benchmark (b). There was also little difference seen when comparing the positions between the present method and the benchmark (c). The agreement between the two graders was better than any other comparison (less than 0.3 pixels difference, on average). Looking at the range of data across the different comparisons, we see the largest range exists for the comparison between the landmark and the benchmark (b; ~14 pixels), while the range was similar for the landmark vs. present method and present method versus benchmark (a and c; ~11 pixels). The range was smallest when evaluating the comparison between graders (d; ~8 pixels). We do not observe and trends for the measurements to become more (or less) different as the average increases. In sum, these plots show that there is reasonable agreement across all measurements.

Reference:

J. M. Bland and D. Altman, "Statistical methods for assessing agreement between two methods of clinical measurement," *The Lancet* i, 307–310 (1986).



Supplementary Figure S6. Eye motion trace segmented into microsaccades and drift.

Microsaccades (green) and drifts (cyan) are shown with blink intervals shown as the dark blue rectangles. Note that refixation periods after each blink are not marked as microsaccades as they have some different characteristics compared to true microsaccades during fixation.

Supplementary Table

Supplementary Table 1. Proportion of tracked frames calculated excluding blinks when using benchmark parameters for the present method

System	Image Quality	Proportion (%) of strips (AOSLO)	Present method	Benchmark
AOSLO	All	Tracked:	98.03%	81.76%
	(n = 30)	Not tracked:	1.97%	18.24%
	High	Tracked:	99.71%	96.69%
	(n = 10)	Not tracked:	0.29%	3.31%
	Medium	Tracked:	96.73%	61.51%
	(n = 10)	Not tracked:	3.27%	38.49%
	Low	Tracked:	97.65%	89.43%
	(n = 10)	Not tracked:	2.35%	10.57%

Supplementary Table 1. Results here are comparable for our method when using the same strip parameters as we used for the benchmark for AOSLO image sequences (15 strips; 64×512 pixel strips). Note that the data here for the benchmark method is identical to that shown in Table 1 in the main manuscript; values are replotted here to ease comparison.